Soliton self-routing in a finite photonic potential

Alessandro Alberucci,[1,*] Chandroth P. Jisha,[2,3] Ray-Kuang Lee,[3] and Gaetano Assanto[1]

[1]*Nonlinear Optics and OptoElectronics Lab (NooEL), Via della Vasca Navale 84, Rome 00146, Italy*

[2]*Centro de Física do Porto, Faculdade de Ciências, Universidade do Porto, R. Campo Alegre 687, Porto 4169-007, Portugal*

[3]*Institute of Photonics Technologies, National Tsing-Hua University, Hsinchu 300, Taiwan*

**Corresponding author: alessandro.alberucci@uniroma3.it*

Received January 16, 2013; revised April 26, 2013; accepted May 8, 2013;
posted May 8, 2013 (Doc. ID 183588); published June 7, 2013

We investigate power-dependent routing of one-dimensional Kerr-like spatial solitons in the presence of a finite photonic potential. Large self-deflections can be obtained using a trapping index well of limited length. © 2013 Optical Society of America

OCIS codes: (190.0190) Nonlinear optics; (190.6135) Spatial solitons; (260.5950) Self-focusing; (260.2710) Inhomogeneous optical media.

http://dx.doi.org/10.1364/OL.38.002071

Optical spatial solitons (OSS) are nonlinear wavepackets that preserve their profile and intensity distribution in propagation: the natural spreading of a light beam due to diffraction is compensated by self-focusing, the latter modeled in Kerr-like media as a dependence of the refractive index n on the beam intensity I, encompassing both local and nonlocal response [1–3]. OSS can also confine other (weaker) signals, thus defining light-induced waveguides and readdressable interconnects whereby the signal propagation path and output location are controlled by the soliton trajectory. To this extent, electro-optic and thermo-optic effect, light-induced perturbations, interfaces and boundaries, parametric as well as collisional interactions have been investigated [3–10], including self-deflection [11–15]. The interaction of OSS and dielectric inhomogeneities, including guiding potentials where solitons tend to oscillate/breathe [16], has been the subject of numerous theoretical analyses, including perturbation theory applied to inverse scattering and equivalent particle or modulation theory [17–24]. Soliton propagation in refractive potentials has recently led to the experimental observation of beam self-steering due to tunnelling [25] or escaping [26].

In this Letter, we investigate the dynamics of spatial solitons launched in a Kerr-like dielectric with a linear refractive potential, which is finite in both longitudinal and transverse dimensions, addressing their power-dependent routing. To this extent we introduce an effective energy accounting for the soliton characteristics, using the Ehrenfest theorem to model self-steering of paraxial OSS over a wide range of deflection angles at the exit of the index perturbation.

For the sake of clarity and simplicity hereby we focus on the paraxial propagation of (1 + 1)D light beams using the generalized nonlinear Schrödinger equation (NLSE) which, in the limit of small perturbations (of both linear and nonlinear origins), reads [2,27]

$$i\frac{\partial u}{\partial Z}+\frac{1}{2}\frac{\partial^2 u}{\partial X^2}-F(|u|^2)u-pV_{\mathrm{eff}}(X,Z)u=0, \qquad (1)$$

with n_0 the unperturbed (background) refractive index. The function F describes the (arbitrary) nonlinear response. An index inhomogeneity acts through the effective potential $V_{\mathrm{eff}}(X,Z)=-2n_0n_L(X,Z)$, with $n_L(X,Z)$ the linear refractive index distribution. w_p is the characteristic width (i.e., along X) of the defect in transverse space. The spatial coordinates are normalized as $Z=z/L_d$ and $X=x/w_p$, with $L_d=k_0w_p^2n_0$ (k_0 is the vacuum wavenumber); we set $p=k_0^2w_p^2/2$.

Let us consider a self-focusing response and a function F, which does not depend explicitly on X and Z, i.e., a homogeneous nonlinearity. Hereafter, we will assume that a fundamental bright soliton is launched at the input $Z=0$ and study its trajectory $\langle X\rangle(Z)=\int\varphi X\mathrm{d}X$, with $\varphi=|u|^2/\int|u|^2\mathrm{d}X$ the normalized wave function. Taking—without loss of generality—$p=1$, the evolution of $\langle X\rangle$ along Z is ruled by the Ehrenfest's theorem [27]

$$\frac{d^2\langle X\rangle}{dZ^2}=-\sum_{m=0}^{\infty}\frac{1}{m!}\left.\frac{\partial^{m+1}U}{\partial X^{m+1}}\right|_{\langle X\rangle}\mu_m, \qquad (2)$$

with $U=V_{\mathrm{eff}}+F(|u|^2)$ the overall potential and $\mu_m=\int(X-\langle X\rangle)^m\varphi\mathrm{d}X$ the centered momentum of order m; we note that $\mu_1=0$ always holds. We limit our analysis to input powers such that the solitons retain their particle-like character [27], i.e., their width is small as compared with w_p. In this regime, if in Eq. (2) we retain terms up to $m=2$, the approximation is expected to be good. Moreover, the solitons conserve their (even) parity with respect to $\langle X\rangle$: Eq. (2) shows that the mean force attributable to $F(|u^2|)$ is zero. Multiplying both sides of Eq. (2) by the beam velocity $v=d\langle X\rangle/dZ$ and integrating between $Z=0$ and Z yields the conservation rule for the equivalent energy E, the latter given by

$$E=\frac{1}{2}v^2+V_{\mathrm{eff}}(\langle X\rangle)+\frac{\mu_2}{2}\left.\frac{\partial^2V_{\mathrm{eff}}}{\partial X^2}\right|_{\langle X\rangle}, \qquad (3)$$

where we neglected changes of OSS waist $\sqrt{\mu_2}$ along Z. In Eq. (3) the terms $(1/2)v^2$ and $V_{\mathrm{tot}}=V_{\mathrm{eff}}+(\mu_2/2)(\partial^2V_{\mathrm{eff}}/\partial X^2)$ represent an equivalent kinetic energy and an equivalent potential, respectively. Equation (3) states that the soliton motion obeys the classical law for point-like particles with the degree of freedom $\langle X\rangle$ and the control parameter $\sqrt{\mu_2}$. The dependence on μ_2

stems from the wave-like nature of OSS [17,27]. In turn, OSS are characterized by a width versus power existence curve, its specific form depending on $F(|u|^2)$. This implies that, when propagating through an inhomogeneous medium, OSS move along power-dependent trajectories owing to differential overlaps with the linear potential.

In order to quantify the soliton dynamics in a specific case, we choose a linear index well of profile $n_L = \Delta \exp(-X^{2l})\mathrm{rect}_d(Z - Z_0 - d/2)$, with $l = 2$ throughout this work. Figure 1(a) plots V_{tot}: for small μ_2 it is $V_{\mathrm{tot}} \approx V_{\mathrm{eff}}$, whereas for increasing soliton waist the flat zone close to $X = 0$ shrinks, with the formation of lateral peaks for larger μ_2. We now examine the role of V_{tot} on the soliton transverse motion, considering input beams launched along Z, i.e., with $v = 0$ at $Z = 0$. The bell-shaped V_{tot} acts as an harmonic oscillator potential, with oscillation period $\Lambda = 2\sqrt{2}\int_0^{X_{\mathrm{in}}} [E(X_{\mathrm{in}}) - V_{\mathrm{tot}}(x)]^{-1/2} dx$ [$X_{\mathrm{in}} = \langle X \rangle (Z = 0)$], thus depending on μ_2 and, via the existence relation, on soliton power. Figure 1(b) illustrates dependence of Λ on both the launch point X_{in} and the soliton width $\sqrt{\mu_2}$. Finally, the soliton trajectories computed from Eq. (2) for $d \to \infty$ (only terms up to $m = 2$ were included) are graphed in Fig. 1(c): noticeably, the oscillations change from sinusoidal to nearly square, due to the strong an harmonicity of the potential V_{tot}. Thus, an efficient power-controlled soliton self-steering can be easily obtained for a finite d, as the output velocity $v_{\mathrm{out}} = v(Z = Z_0 + d)$ depends on power according to

$$v_{\mathrm{out}} = \pm\sqrt{2[V_{\mathrm{out}}(X_{\mathrm{in}}) - V_{\mathrm{tot}}(X_{\mathrm{out}})]}, \tag{4}$$

where $X_{\mathrm{out}} = \langle X \rangle (Z = Z_0 + d)$ is the soliton position at the exit of the linear perturbation n_L.

Although up to now all the results were independent from the specific form of $F(|u|^2)$, the specific nonlinear response comes into play when assessing the validity range of our approach. For the sake of discussion, we focus hereafter on the simplest case of a local Kerr nonlinearity $F = |u|^2$ and a fundamental bright soliton $u(X) = u_0\,\mathrm{sech}(u_0 X)$ [2]. Figure 1(b) graphs the oscillation period Λ computed from Eq. (1) with the aid of the beam-propagation method, taking a soliton input profile and varying its width $\sqrt{\mu_2}$ (given by $0.907/u_0$ for sech-like beams) and input position X_{in}; Fig. 2 shows a selection of the corresponding intensity profiles on the plane XZ. For small widths, the numerical results nearly coincide with the theoretical predictions of Eq. (3): the nonlinear response dominates, with negligible changes in soliton size versus propagation. For $\sqrt{\mu_2} > 0.1$, the transverse size of the intensity distribution becomes comparable with the size w_p of the linear potential V_{eff}: an appreciable amount of power couples to radiation modes of the linear guide, causing a discrepancy between theory and numerics. Moreover, the coherent interaction of radiated and self-confined waves yields a complex aperiodic behavior right after the input section, although periodic oscillations are restored for large Z. For $\sqrt{\mu_2} > 0.5$, the period Λ tends to the same value for every X_{in}: in this limit the soliton feels a mean potential stemming from the average of V_{eff} across its own profile, disregarding the local details of the mutual overlap versus propagation coordinate.

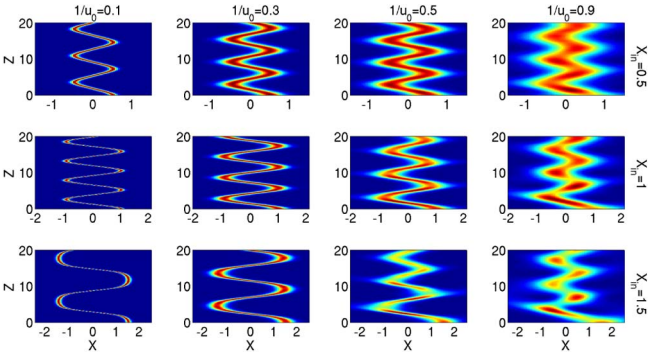

Fig. 2. Soliton oscillations in a trapping well infinitely extended across Z, versus input radius $1/u_0$ and initial position X_{in}, computed via BPM code solving Eq. (1). Here $\Delta = 1$.

Equation (4) clearly states that the soliton exit angle depends on the longitudinal extent of the index perturbation. To focus on power control, hereby we set $d = 10$. The evolution of beams with various amplitudes propagating through an index perturbation with $Z_0 = 2$ are displayed as an overlay in Fig. 3, the coarser the contour plot the higher the input power. The exit angles of the OSS from the linear well span both upper and lower halves of the output plane as input power varies, while

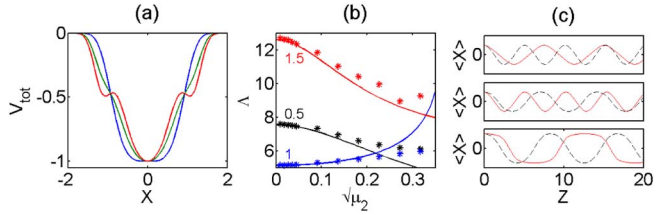

Fig. 1. (a) Overall potential V_{tot} versus X for $\sqrt{\mu_2} = 0.001$, 0.3, and 0.4, larger μ_2 correspond to a narrower lobe around the center $X = 0$. (b) Oscillation period versus soliton width $\sqrt{\mu_2}$ computed from Eq. (2) (solid lines) and from Eq. (1) (symbols); the numbers next to each line indicate the corresponding initial position X_{in}. (c) Soliton trajectories in an infinitely extended potential ($d \to \infty$), and for $X_{\mathrm{in}} = 0.5$, 1, and 1.5, from top to bottom, respectively; solid and dashed lines correspond to $\sqrt{\mu_2} = 0.001$ and 0.2, respectively. Here $\Delta = 1$.

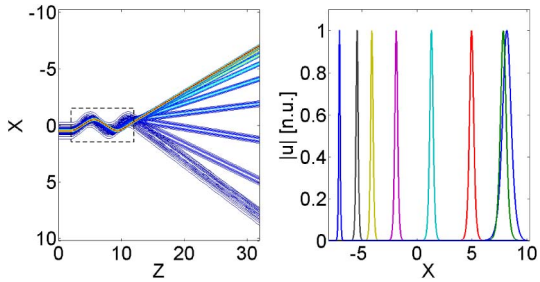

Fig. 3. Left: beam evolution for input amplitudes ranging from $u_0 = 2$ to $u_0 = 12$; $d = 10$ and the input position is $X_{\mathrm{in}} = 0.5$ (the dashed rectangle indicates the linear index well). Right: corresponding output profiles normalized to their peak value from $u_0 = 8$ to $u_0 = 2$, from left to right, respectively. Here we set $\Delta = 1$.

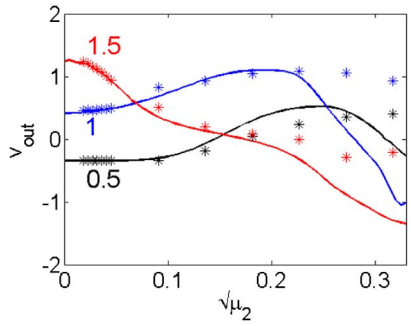

Fig. 4. Theoretical (solid lines) and numerical (points) predictions for the soliton output velocity v_{out} versus input width $\sqrt{\mu_2}$, for various input positions X_{in} (labels next to each line). Here $d = 10$ and $\Delta = 1$.

the self-trapped nature of the beams is preserved. Figure 4 shows the exit angle versus soliton width $\sqrt{\mu_2}$ for three input positions X_{in}, as obtained from numerical simulations of (1) and theoretical prediction from (2). The agreement is similar to the case of the oscillation period Λ plotted in Fig. 1.

Figure 4 demonstrates also the operation of an all-optical router where the location of the signal output is determined by either power or position (or both) of the injected soliton. For the range of initial waists considered in the figure, nearly all the launched power transfers to the output soliton, with a maximum coupling loss of about 2%. Noteworthy, in physical units the deflection angle is given by $\arctan[v_{\mathrm{out}}/(k_0 n_0 w_p)]$. If we take $n_0 \approx 1.4$ and reminding $p = 1$, $v_{\mathrm{out}} \approx 1$ corresponds to an actual deflection angle of $\approx 26°$; we stress that for deflection angle larger than 30° nonparaxial effects need to be accounted for. Finally, the use of nonlinearity in soft matter, e.g., a nonlocal reorientational response, would permit sub-mW excitation of spatial solitons in two transverse dimensions and ensure their stability and self-confinement over a broad range of launch conditions [3].

In conclusion, we investigated the propagation of OSS in linear potentials of finite extent. We introduced an equivalent energy to describe the soliton motion, accounting for the beam overlap with the linear index distribution. Our model describes well the dependence of the soliton trajectory on excitation. For finite-length trapping potentials it is possible to control the soliton emission over a broad angular range, thus realizing a novel and effective power-driven signal router.

JCP and AA acknowledge grant support from the FCT SFRH/BPD/77524/2011 and from Regione Lazio, respectively.

References

1. G. I. Stegeman and M. Segev, Science **286**, 1518 (1999).
2. Y. S. Kivshar and G. P. Agrawal, *Optical Solitons* (Academic, 2003).
3. M. Peccianti and G. Assanto, Phys. Rep. **516**, 147 (2012).
4. W. E. Torruellas, G. Assanto, B. L. Lawrence, R. A. Fuerst, and G. I. Stegeman, Appl. Phys. Lett. **68**, 1449 (1996).
5. L. Friedrich, G. I. Stegeman, P. Millar, C. J. Hamilton, and J. S. Aitchison, Opt. Lett. **23**, 1438 (1998).
6. B. Alfassi, C. Rotschild, O. Manela, M. Segev, and D. N. Christodoulides, Opt. Lett. **32**, 154 (2007).
7. C. Rotschild, B. Alfassi, O. Cohen, and M. Segev, Nat. Phys. **2**, 769 (2006).
8. A. Alberucci, A. Piccardi, U. Bortolozzo, S. Residori, and G. Assanto, Opt. Lett. **35**, 390 (2010).
9. Y. V. Izdebskaya, V. G. Shvedov, A. S. Desyatnikov, W. Krolikowski, and Y. S. Kivshar, Opt. Lett. **35**, 1692 (2010).
10. A. Piccardi, A. Alberucci, R. Barboza, O. Buchnev, M. Kaczmarek, and G. Assanto, Appl. Phys. Lett. **100**, 251107 (2012).
11. A. E. Kaplan, JETP Lett. **9**, 33 (1969).
12. A. T. Ryan and G. P. Agrawal, Opt. Lett. **18**, 1795 (1993).
13. F. Ye, Y. V. Kartashov, B. Hu, and L. Torner, Opt. Lett. **34**, 2658 (2009).
14. A. Piccardi, A. Alberucci, and G. Assanto, Appl. Phys. Lett. **96**, 061105 (2010).
15. A. Piccardi, A. Alberucci, and G. Assanto, Phys. Rev. Lett. **104**, 213904 (2010).
16. M. Peccianti, A. Fratalocchi, and G. Assanto, Opt. Express **12**, 6524 (2004).
17. A. B. Aceves, J. V. Moloney, and A. C. Newell, Phys. Rev. A **39**, 1809 (1989).
18. Y. S. Kivshar and B. A. Malomed, Rev. Mod. Phys. **61**, 763 (1989).
19. S. Garzia, C. Sibilia, and M. Bertolotti, Opt. Commun. **139**, 193 (1997).
20. Y.-D. Wu, Opt. Express **12**, 4172 (2004).
21. A. Fratalocchi and G. Assanto, Opt. Lett. **31**, 1489 (2006).
22. L. W. Dong and H. Wang, Appl. Phys. B **84**, 465 (2006).
23. G. Assanto, A. A. Minzoni, M. Peccianti, and N. F. Smyth, Phys. Rev. A **79**, 033837 (2009).
24. G. Assanto, N. F. Smyth, and W. Xia, Phys. Rev. A **84**, 033818 (2011).
25. A. Barak, O. Peleg, C. Stucchio, A. Soffer, and M. Segev, Phys. Rev. Lett. **100**, 153901 (2008).
26. M. Peccianti, A. Dyadyusha, M. Kaczmarek, and G. Assanto, Phys. Rev. Lett. **101**, 153902 (2008).
27. C. P. Jisha, A. Alberucci, R.-K. Lee, and G. Assanto, Opt. Lett. **36**, 1848 (2011).